Power density improvement of axial flux permanent magnet synchronous motor by using different magnetic materials

Mohamed Amine Hebri, Abderrahmane Rebhaoui, Gregory Bauw, Jean-Philippe Lecointe, Stéphane Duchesne, Gianluca Zito, Abdelli Abdenour, Victor Mediavilla Santos, Vincent Mallard, Adrien Maier

POWER DENSITY IMPROVEMENT OF AXIAL FLUX PERMANENT MAGNET SYNCHRONOUS MOTOR BY USING DIFFERENT MAGNETIC MATERIALS

Mohamed Amine Hebri
Univ. Artois, UR 4025, Laboratoire Systèmes Electrotechniques et Environnement, Béthune, F-62400, France
e-mail: mamine.hebri@univ-artois.fr

Abderrahmane Rebhaoui
Institut VEDECOM - Versailles, 78000, France

Grégory Bauw
Univ. Artois, UR 4025, Laboratoire Systèmes Electrotechniques et Environnement, Béthune, F-62400, France

Jean-Philippe Lecointe
Univ. Artois, UR 4025, Laboratoire Systèmes Electrotechniques et Environnement, Béthune, F-62400, France

Stéphane Duchesne
Univ. Artois, UR 4025, Laboratoire Systèmes Electrotechniques et Environnement, Béthune, F-62400, France

Gianluca Zito
IFP Energies Nouvelles, Rueil-Malmaison, 92852, France.

Abdenour Abdelli
IFP Energies Nouvelles, Rueil-Malmaison, 92852, France.

Victor Mediavilla Santos
IFP Energies Nouvelles, Rueil-Malmaison, 92852, France.

Vincent Mallard
CRITT M2A, Bruay-la-Buissière, 62700, France

Adrien Maier
EREM - Etudes Réalisations Et Maintenance, Wavignies, F-60130, France

Abstract

Design/methodology/approach – This paper presents a study to improve the power density and efficiency of e-motors for electric traction applications with high operating speed. The studied machine is a yokeless-stator axial flux permanent magnet synchronous motor with a dual rotor. The methodology consists in using different magnetic materials for an optimal design of the stator and rotor magnetic circuits to improve the motor performance. The candidate magnetic materials, adapted to the constraints of eMobility, are made thin laminations of Si-Fe Non-Oriented grain Electrical Steel (NOES), Si-Fe Grain-Oriented Electrical Steel (GOES) and Iron-Cobalt Permendur electrical steel (Co-Fe).
Purpose – The main objective is to exploit the optimal performances of each magnetic material in terms of low iron losses and high saturation flux density, in order to improve the efficiency and the power density of the selected motor.
Findings – The mixed GOES-CoFe structure allows to reach 10kW/kg in rated power density and a high efficiency in city driving conditions. This structure allows to make the powertrain less energy consuming in the Battery Electric Vehicles, and to reduce CO_2 emissions in Hybrid Electric Vehicles.
Originality/value – The originality of this study lies in the improvement of both power density and efficiency of the electric motor in automotive application by using different magnetic materials through a multi-objective optimization.
Keywords – Axial flux machines, Multiobjective optimization, Optimal design, Permanent magnet machine, Soft magnetic materials.
Paper type – Research paper

I. INTRODUCTION

The road transport sector is a major source of greenhouse gas emissions, including CO_2. For this reason, new restrictions and limitations of the CO_2 emissions are implemented by the European Union in order to reach carbon neutrality in 2050 *(Auverlot et al., 2018*). For example, in Europe and in 2020, CO_2 emissions are limited to 95g/km on average for new cars (*Auverlot et al., 2018*). This context leads car manufacturers to reduce their environmental impact in order to avoid penalties when the emissions exceed defined thresholds. As a result, and for several years, these manufacturers have been offering in their ranges Hybrid Electric Vehicles (HEV), Plug-in Hybrid Electric Vehicles (PHEV), and Battery Electric Vehicles (BEV) (*Chan, 2002*). To make these cars economic and efficient, the manufacturers have the objective to improve the efficiency of the whole electric powertrain (*Chan, 2002; Auverlot et al., 2018; Cisse et al., 2018*).

Improving efficiency requires to reduce losses in each element of the powertrain, as well as reducing its energy consumption due to the total weight of the components (*Chan, 2002*). This paper focuses on the electric motor by improving its efficiency and power to weight ratio. In automotive traction applications, the radial flux Permanent Magnet Synchronous Motors (PMSMs) are generally used due to its high-power density, high efficiency, compact size and manufacturing simplicity (*Hanselman, 1994; Cisse et al., 2018; Zhu and Howe, 2007*). Axial flux PMSMs are good candidate as their power density may be even higher (*Campbell, 1974; Gieras et al., 2008*). There are different topologies depending on the number of rotors and stators (*Amin et al., 2019*). To further improve the power density of axial-flux PMSM, there are several ways:

- the current density can be increased, but is limited by the thermal constraints and the cooling system (*Laidoudi et al., 2020; Pyrhonen et al., 2008*);
- the maximum rotation speed can be increased, but is limited by mechanical constraints: the peripheral speed and the transmission system (*Borisavljevic, 2013; Pyrhonen et al., 2008; Rezzoug and El Hadi Zaïm, 2012*);
- the use of permanent magnets with very high energy density are recommended (NdFeB, SmCo) (*Dwivedi et al., 2006; Nagorny et al., 2005*) but their environmental footprint is non-negligible;
- the use of magnetic materials with high permeability, high saturation flux density and low specific losses is also a way to analyse, as Grain-Oriented Electrical Steel (GOES) or Iron-Cobalt Permendur electrical steel (CoFe) (*Bloch et al., 2007; Kowal et al., 2010; Rebhaoui et al., 2022b*).

In this paper, the authors analyze the impact of using different electrical steels in the magnetic circuit of a yokeless-stator dual-rotor axial flux PMSM. Conventionally, electric motors for automotive applications are designed with Non-Oriented grain Electrical Steel (NOES), which are well suited for rotating field applications (*Pyrhonen et al., 2008*). In this work, other magnetic materials are used as GOES. The latter is commonly applied in power transformer magnetic circuits (*Fujisaki, 2019; Pyrhonen et al., 2008*); it is characterized by a very high magnetic permeability, a high saturation flux density and low specific losses, compared to the conventional NOES. Similarly, Permendur CoFe, which is commonly used in aeronautical applications, is an attractive candidate due to its very high saturation flux density compared to NOES and GOES (*Bloch et al., 2007; Fujisaki, 2019*). The high level of saturation allows to reduce the size of the stator teeth and rotor yoke and, thus, to increase the power density at iso-torque (*Bhagubai and Fernandes, 2020*). The low specific losses increase the efficiency of the machine (*Rebhaoui et al., 2022b*).

The paper is separated in four sections. First, a comparison between different candidate magnetic materials for e-mobility is presented, in terms of B-H curves (permeability and flux density level at saturation) and specific losses. Second, the studied motor is presented in its complete form and its equivalent 2-D Finite Element model, as well as the main parameters. In addition, the design approach and the integration of materials are explained. A presentation of the software and the simulation parameters is proposed. Third, the FEA numerical calculations results are presented in the form of mono-objective and multi-objective optimizations. According to the reference (*Pyrhonen et al., 2008*), a current density of 13-18A/mm² can be reached in the stator winding with water cooling. In a first step, an operating point has been chosen with high current density (15A/mm²) to achieve a high-power density, the purpose of this study is to quantify the gain of using different magnetic materials for this operating point. Fourth, the main results corresponding to power density, iron losses, and efficiency are presented and discussed. Using a multi-objective optimisation, a structure was chosen. On this structure, the performance of the motor in the torque/speed plane has been performed using the MTPA (Maximum Torque Per Ampere) control strategy. In addition, a thermal study is performed on this motor. The article will be ended with a conclusion.

II. MAGNETIC MATERIALS

Fig. 1-a shows the B-H curves for the three magnetic materials analyzed in this paper: NOES (*ArcelorMittal Electrical Steel, 2022*), GOES (*Thyssenkrupp Electrical Steel GmbH, 2022)* and the Permendur Hiperco50 (*Carpenter Electrification, 2022*), which thicknesses are 0.20mm, 0.20mm and 0.15mm respectively. The measurements are obtained with a standardised Single Sheet Tester (SST) frame at 50 Hz. SMC materials have not been selected because of their low saturation flux density and low permeability.

The curves show that the GOES strips magnetized along the Rolling Direction (RD) have a high maximal permeability, about 31000, over 2 times more compared to NOES and Permendur (Fig. 1-b). On the other hand, GOES is highly anisotropic, which means that the performances in the Transverse Direction (TD) are much less interesting. The Permendur Hiperco50 sheet has a high saturation flux density value, over 2.25T, versus 1.83T for the conventionnel NOES and 2.03T for the GOES magnetized along the RD (Table I).

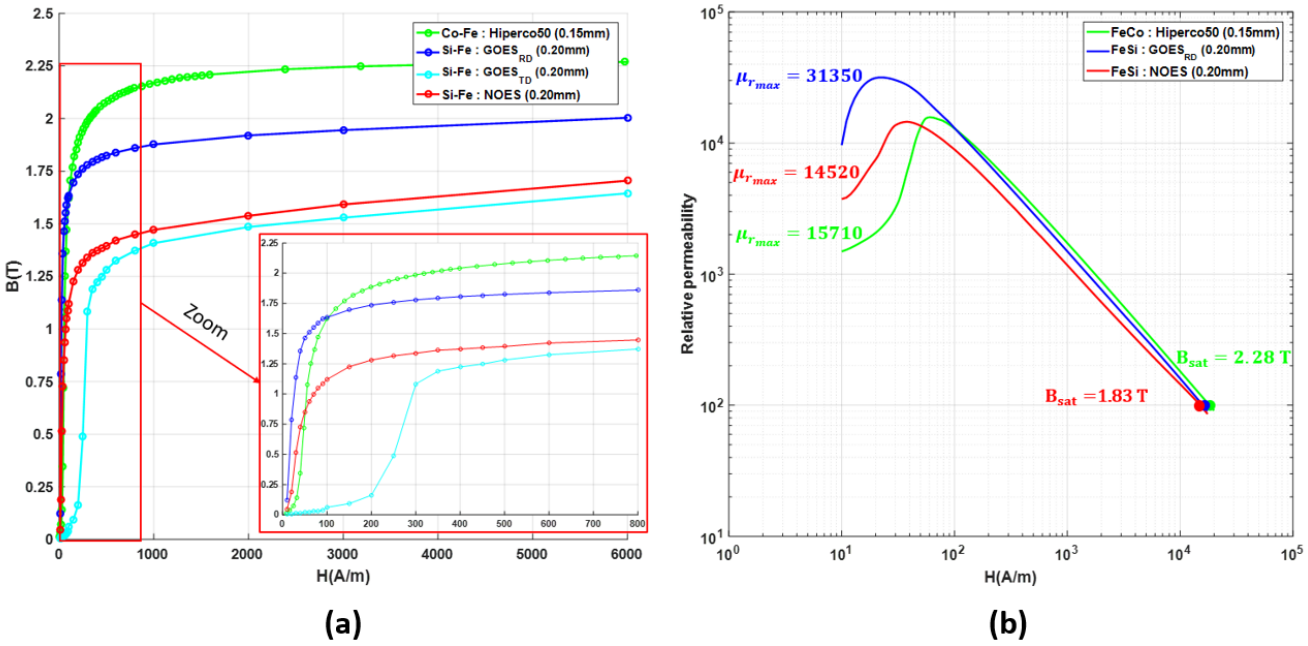

Fig.1. Performance of the different magnetic sheets used at 50Hz: a) B-H curves, b) relative permeability

TABLE I
MAGNETIC PROPERTIES

	Saturation flux density @ μ_r=100	Maximal relative permeability	Mass density
3% Si-Fe - NOES	1.83 T	14520	7650 kg/m^3
3% Si-Fe - GOES	2.03 T	31350	7650 kg/m^3
Co-Fe : Hiperco50	2.28 T	15350	8120 kg/m^3

Fig. 2 shows the specific losses for the different magnetic sheets when frequency is 500Hz. The GOES sheet magnetized along the RD presents the lowest iron losses, compared to the conventional NOES sheet, at iso-thickness.

In parallel, GOES strips of 0.20mm thickness have iron losses almost equal to the Co-Fe losses strips of 0.15mm thickness, at 500Hz and for flux density values lower than 1.8T. On the other hand, the performances of the GOES sheet following the TD are not interesting anymore. The Permendur Hiperco50 steel becomes advantageous for the high frequency operating ranges because of its low thickness which limits the eddy current losses in the laminations.

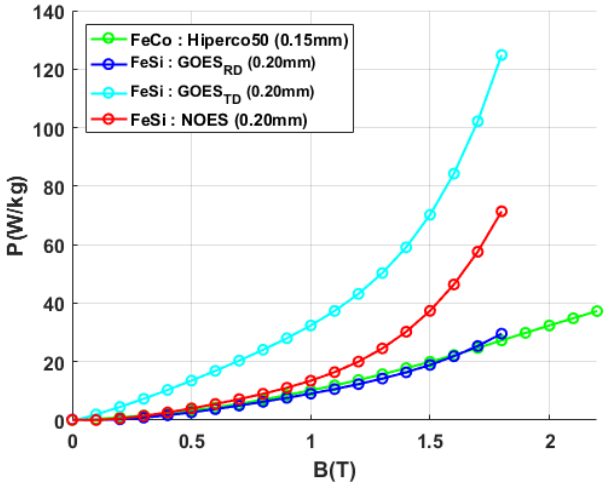

Fig.2. Specific losses for the different magnetic sheets used at 500Hz

III. DESIGN APPROACH

The studied axial flux dual-rotor and yokeless-stator PMSM is shown in Fig. 3-a. In order to simplify the study and the modelling, the authors has modelled a 2D structure at the average radius (Fig. 3-b) of the axial flux PMSM. The main motor parameters are presented in Table II.

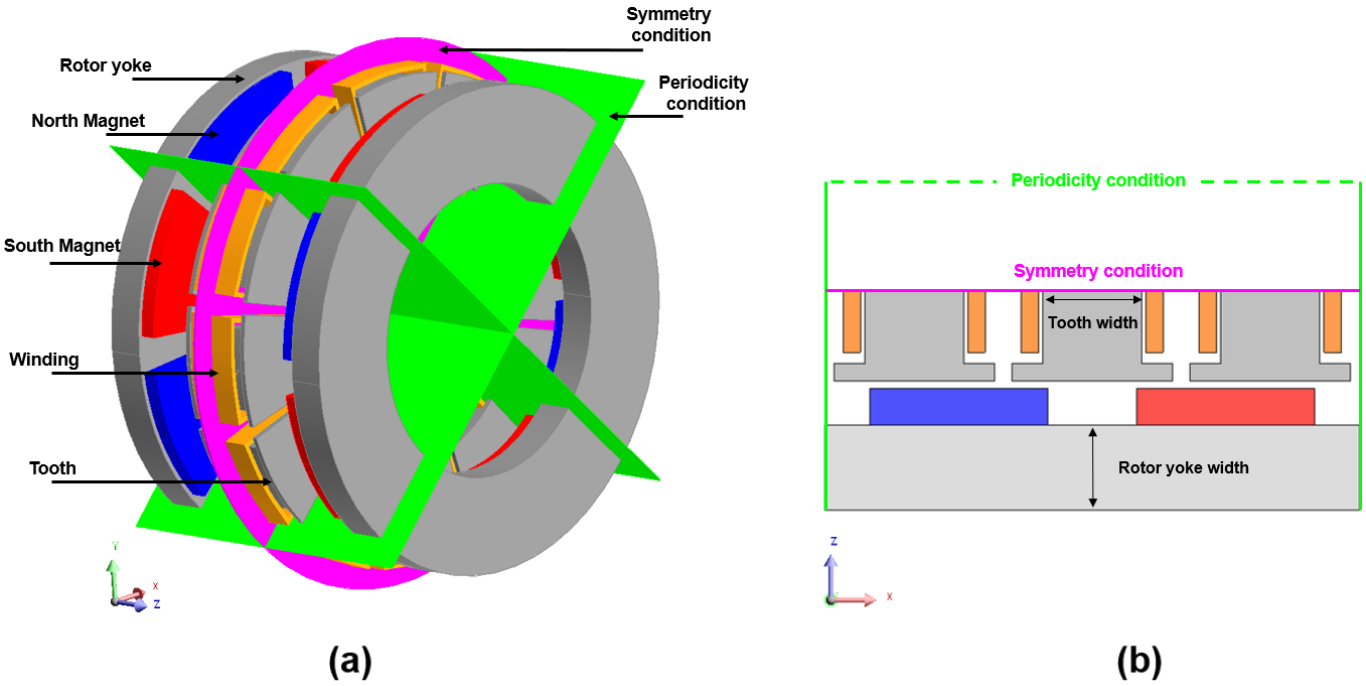

Fig.3. The PMSM structure studied: a) in 3D, b) in 2D at average radius

TABLE II
MOTOR PARAMETERS

Slot / Pole number	12 / 8
Inner / Outer radius	60mm / 100mm
Base rotational speed	10000rpm
Number of series turns per phase	60
Rated current	130Arms
Airgap	1.3mm
Magnet width	6.5mm

To improve power density and efficiency of the active parts of the studied axial flux, the authors propose to analyse the impact of using non-conventional materials for the magnetic stator and rotor circuits. The strategy relies on the intrinsic properties of these materials but also on the topology of the magnetic circuit:

- It can be taken advantage of the Hiperco50 low thickness of 0.15mm to reduce the iron losses (eddy current losses) and consequently to improve the efficiency. Its high saturation flux density allows to reduce the size of the circuits;
- GOES has good performance in the RD, which is usable in the stator teeth where the field lines are quasi-unidirectional along the axial direction. The fig. 4 shows that the flux density in the teeth is mainly oriented along the rolling direction of the lamination, *ie* in the direction of the teeth. That is the case whatever the rotor position as the grain oriented tends to drive the flux in the easy magnetization direction for which the permeability is the highest. In the tips, the field lines distribution depend on the rotor position; therefore the transverse direction can be more or less solicited, impacting the iron losses;
- In the rotor yoke, despite the rotating direction of the field (Fig. 4), possibility of using GOES can be studied.

The geometric parameters which are optimized are the yoke width and the tooth width, respecting the necessary slot area for the wire arrangement, as well as the saturation levels of the sheets. The aim is to find the optimal geometrical dimensions for a high-power density, in the power range between 90kW and 105kW, at a given rotational speed of 10 000rpm and at a given current density ($15A_{rms}/mm^2$). The power density $P_{density}$ is defined as the ratio between the power and the total mass of the active parts of

the machine (magnet mass "m_{magnet}", winding mass "$m_{winding}$" (considering the end winding), stator teeth mass "m_{teeth}", and rotor yokes mass "$m_{rotor-yoke}$"). The power density is written:

$$P_{density} = \frac{\omega_r \times T}{m_{magnet} + m_{teeth} + m_{rotor-yoke} + m_{winding}} \quad (1)$$

where ω_r is the angular velocity in (*rad/s*) and T is the electromagnetic torque in (*N.m*).

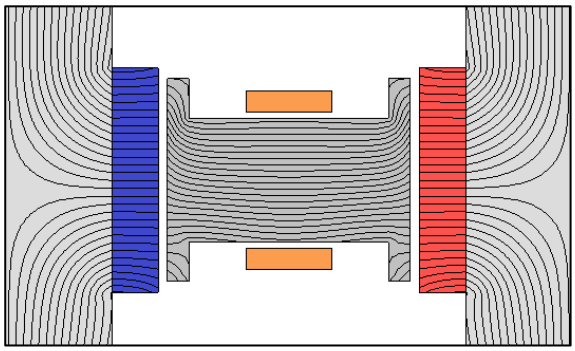

Fig.4. Flux lines in a pole of axial flux PMSM

The 3 magnetic materials described in Fig.1 are combined in the stator teeth and the rotor yoke, which lead to 9 configurations of magnetic circuits described in Table III.

TABLE III
COMBINATIONS FOR THE MAGNETIC CIRCUITS

Structure names	Tooth material	Yoke material
Tn-Yn	NOES	NOES
Tn-Yg	NOES	GOES
Tn-Yh	NOES	Hiperco50
Tg-Yn	GOES	NOES
Tg-Yg	GOES	GOES
Tg-Yh	GOES	Hiperco50
Th-Yn	Hiperco50	NOES
Th-Yg	Hiperco50	GOES
Th-Yh	Hiperco50	Hiperco50

IV. FEA-2D MODELING

The numerical modeling is based on a Finite Element Analysis (FEA) using the commercial JMAG-Designer Ver.20.1 software. The software is a Powersys product, and it was released in May 2021. This software application allows to take into account both magnetic circuit saturation and magnetic anisotropy when GOES is modelled. Modelling the magnetic permeability tensor should take into account the non-linear interactions in all the magnetization directions; it is practically modelled with a diagonal permeability tensor based on measurements of the magnetic characteristics in RD and TD (*JMAG, 2022*).

$$B = \begin{bmatrix} \mu_x & 0 \\ 0 & \mu_y \end{bmatrix} \times H \quad (2)$$

where B is the flux density in Tesla (*T*), H is the magnetic field in (*A/m*), and μ_x, μ_y are the permabilities in (*H/m*) in the RD and TD directions, respectively.

The calculation of iron losses is performed using the classical approximation of the Steinmetz model which is based on standardized measurements. For GOES, the same model is used with bidirectional coefficients and it also takes into account the harmonics (*JMAG, 2022*):

$$P_{core\_loss} = \sum_{i=1}^{N} \begin{cases} \left(K_{h_{RD}}.\ B_{RD}^{\alpha} + K_{h_{TD}}.\ B_{TD}^{\alpha}\right).f^{\beta} \\ + \\ \left(K_{e_{RD}}.\ B_{RD}^{\gamma} + K_{e_{TD}}.\ B_{TD}^{\gamma}\right).f^{\delta} \end{cases} \quad (3)$$

where i is the harmonic rank, N is the highest harmonic, f is the operating frequency in (*Hz*), B_{RD}, B_{TD} are the maximum level of flux densities according to the RD and TD in (*T*). The coefficients K_h, K_e, α, β, γ, and δ are determined with the measurement data.

The boundary conditions allow to reduce the geometry of the machine. The periodicity condition reduces the machine to 3 slots/2 poles (1/4 machine) and the symmetry condition allows to study the machine with one rotor and one half stator (Fig. 5). This reduces the computational time. The mesh of 9304 elements is shown in Fig. 5. The airgap is divided in 3 layers to get a good accuracy of the flux density.

An HP Z600 workstation 2x Intel Xeon X5650 6-Core 2.66GHz 48GB RAM is used for the simulation.

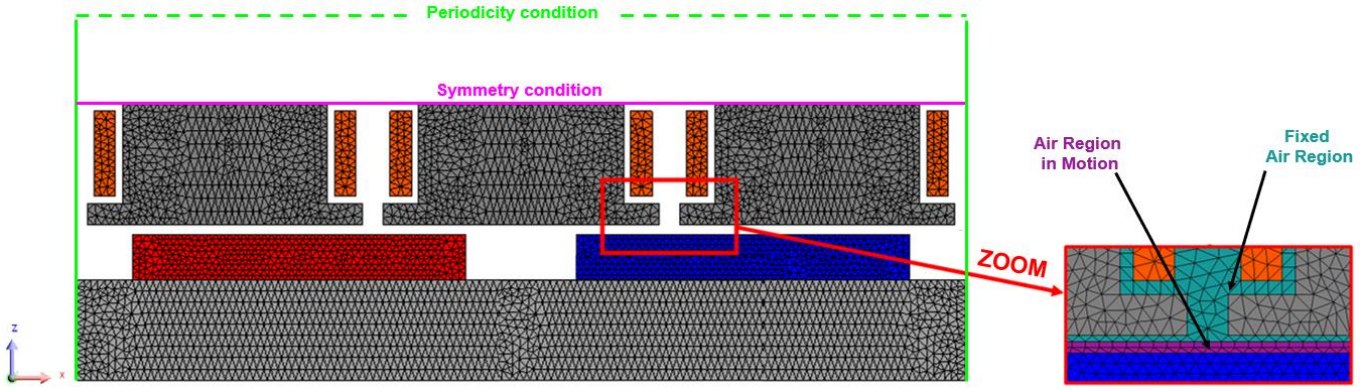

Fig.5 Mesh of the studied structure

IV. FEA-2D RESULTS

A. Parameter variations and reference results:

In this part, the numerical results of the structures presented in table III are shown. A comparison of the power densities, iron losses, and efficiencies between the different structures according to the different magnetic materials and the geometrical dimensions of the stator teeth and the rotor yoke is shown in Fig. 6, 7 and 8. The variation range and step of the yoke thickness and the tooth width are respectively from 9 to 16mm with 1mm spacing and from 19 to 29mm with 0.5mm spacing. The area required for the conductors is taken into account. These limits varied depending on the magnetic material used in each structure, in order to satisfy the saturation flux density constraint in and the power range between 90 and 105kw.

The power density calculation only considers the active parts in the weight calculation. The efficiency calculation takes into account the iron losses, magnet losses and Joule losses considering the end coils and the skin effect/proximity effect.

The time needed for all the simulations is about 1 hour.

For the full NOES conventional reference structure (Tn-Yn), the maximum power density is 9.39kW/kg obtained with a 24mm tooth width and a 12mm yoke width (Fig. 6-a). For the same structure, the maximum efficiency is 98.14%, obtained with a tooth width of 29mm and a rotor yoke width of 16mm (Fig. 7-a).

B. Power density optimization:

The Table IV and Fig. 6 allow to draws the following conclusions about the power density modifications :

- Keeping the NOES sheet in the rotor yoke, the stator teeth is replaced with non-conventional magnetic materials:
  - The use of GOES and Hiperco50 sheets in the stator teeth allows to improve the power density. GOES (Tg-Yn) leads to obtain a maximum power density of 9.57kW/kg, 2% more compared to the reference structure and with a yoke width of 12mm and a tooth width of 22mm (Fig. 6-d);
  - The use of the Hiperco50 sheet (Th-Yn) increases the power by 1.9% (9.56kW/kg) with a yoke thickness of 11mm and a tooth width of 19mm (fig. 6-g).
- Keeping the NOES in the stator teeth and replacing the rotor yoke with GOES and Hiperco50 also allow to improve the power density:
  - By using the GOES (Tn-Yg), the maximum power density is 9.74kW/kg, i.e. an increase of 3.7%, with a yoke width of 11mm and a tooth width of 24mm (Fig. 6-b);
  - Hiperco50 (Tn-Yh) leds to a maximum power density of 9.91kW/kg, with yoke width of 11mm and a tooth width of 19mm (fig. 6-g).
- When non-conventional materials is in both stator and rotor magnetic circuits:
  - the Full GOES structure allows to have a maximum power density of 9.94kW/kg for a yoke width of 11mm and a tooth width of 22mm;

- A full Hiperco50 structure can give a max power density of 10.09kW/kg for a yoke width of 10mm and a tooth width of 20mm.

- For non-conventional mixed structures:
  - GOES teeth and a Hiperco50 yoke lead to a power density of 10.11kW/kg for a yoke width of 10mm and a tooth width of 22mm
  - Hiperco50 teeth and a GOES yoke provide 9.92kW/kg for a yoke width of 11mm and a tooth width of 20mm.

The use of Hiperco50 sheets in the rotor yoke is more advantageous than NOES and GOES sheets. The best structures in terms of power density improvement are the mixed structure with GOES teeth and Hiperco50 yoke and the full Hiperco50 structure.

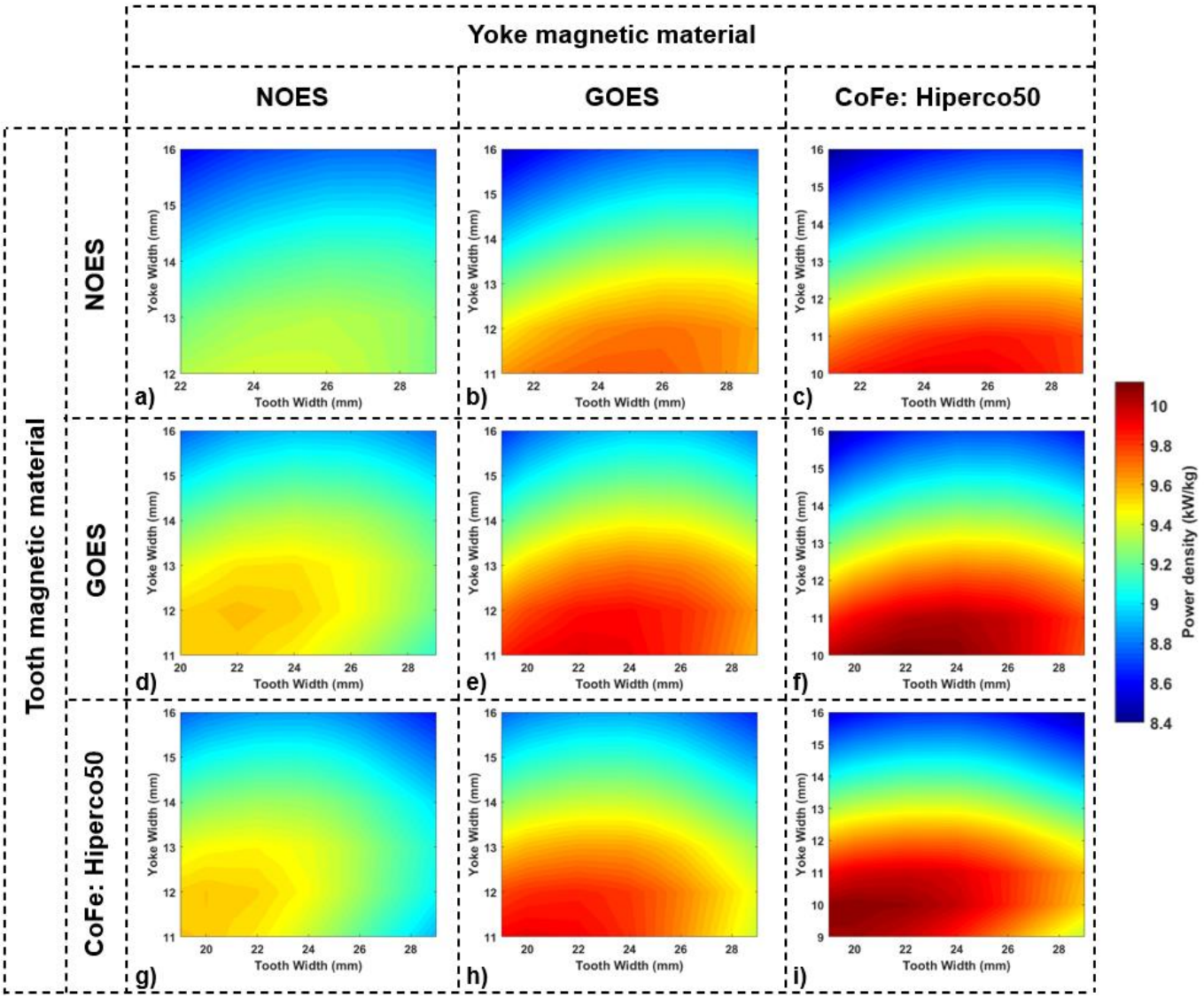

Fig.6. Variation of power density as a function of the tooth width and the yoke width for: a) Tn-Yn, b) Tn-Yg, c) Tn-Yh, d) Tg-Yn, e) Tg-Yg, f) Tg-Yh, g) Th-Yn, h) Th-Yg, i) Th-Yh

TABLE IV
MAXIMAL POWER DENSITIES AND GAIN

Structures	Max power density (kW/kg)	Gain (%)
Tn-Yn	**9.39**	**-**
Tn-Yg	9.74	3.72
Tn-Yh	9.91	5.53
Tg-Yn	9.57	1.91
Tg-Yg	9.94	5.85
Tg-Yh	10.11	7.66
Th-Yn	9.56	1.81
Th-Yg	9.92	5.64
Th-Yh	10.09	7.45

A 3D study was carried out to validate the 2D modelling approach in terms of power density calculations. The 3D calculations lasted 408 hours. Table V gives the differences between the 3D and 2D calculations. The average difference varies from 1.37% for the Tn-Yn structure up to 2.25% for the Tg-Yg and Th-Yh structures. The 2D results are always underestimated compared to the 3D results. The overall average difference for 580 simulation cases is 2.06%, which allow to conclude that the 2D model is enough accurate to establish a reliable design.

TABLE V
DIFFERENCE BETWEEN THE FEA-3D AND FEA-2D

Structures	Minimum difference (%)	Maximum difference (%)	Average difference (%)	Number of simulation cases
Tn-Yn	1.03	2.14	1.37	40
Tn-Yg	2.13	2.74	2.38	54
Tn-Yh	1.12	2.18	1.57	63
Tg-Yn	1.42	3.74	2.05	60
Tg-Yg	1.60	2.82	2.25	66
Tg-Yh	1.54	2.86	2.03	77
Th-Yn	1.48	4.04	2.14	66
Th-Yg	1.59	4.18	2.16	66
Th-Yh	1.59	4.17	2.25	88

C. Iron losses

From figure 7, we can see that the change in the magnetic material of the rotor yoke does not strongly affect the iron losses, this is mainly due to the very low iron losses in the rotor, as the frequency of the magnetic field in the rotor isclose to zero. For example, the minimum iron losses for the Tn-Yn, Tg-Yn, Tf-Yn structures are 252.03W, 254.11W, 181W respectively. By changing the common rotor material from NOES to Hiperco50, the iron losses are respectively 258.84W, 260.30W, and 183.80W. We can say that we have the same iron losses with negligible differences. However, the use of GOES sheet in the rotor slightly increases the iron losses than the Hiperco50 and NOES because the magnetic field flows in the direction of difficult magnetisation. For example, the minimum iron losses for the Tn-Yn, Tg-Yn, Tf-Yn structures are 260.59W, 268.50W, 186.2W respectively.

Furthermore, we notice that the change of the stator tooth material has a very significant impact on the iron loss value. For example, for a tooth width of 22mm and a yoke thickness of 12mm, for the full NOES structure (Tn-Yn) the value of the iron losses is 323.23W, by replacing the tooth with GOES and Hiperco50 teeth, we obtain iron losses of 290.42W and 217.72W respectively, i.e. reductions of 18.18% and 32.66%. These reduction values can show the impact of using such magnetic materials (GOES and Hiperco50) on iron losses.

The use of cobalt iron (Hiperco50) is the most advantageous in terms of iron loss in the teeth. This is obvious, because it has the lowest specific losses compared to NOES and GOES.

From Table VI, it can be seen that the average difference in iron losses between 2D and 3D simulations varies from 7.99% for the structure Tn-Yh to 11.74% for the structure Th-Yn. The 2D results are always underestimated compared to the 3D calculation. The overall average difference for 257 simulation cases is 10.30%. For GOES sheet structures, the iron losses cannot be calculated in JMAG V20.2, due to calculation divergence. Therefore, we cannot make a comparison but it is clear that the 2D model is not accurate for computing the iron losses.

TABLE VI
DIFFERENCE BETWEEN THE FEA-3D AND FEA-2D

Structures	Minimum difference (%)	Maximum difference (%)	Average difference (%)	Number of simulation cases
Tn-Yn	6.55	10.93	8.50	40
Tn-Yg	-	-	-	54
Tn-Yh	5.99	11.00	7.99	63
Tg-Yn	-	-	-	60
Tg-Yg	-	-	-	66
Tg-Yh	-	-	-	77
Th-Yn	9.33	15.82	11.74	66
Th-Yg	-	-	-	66
Th-Yh	8.78	16.98	11.70	88

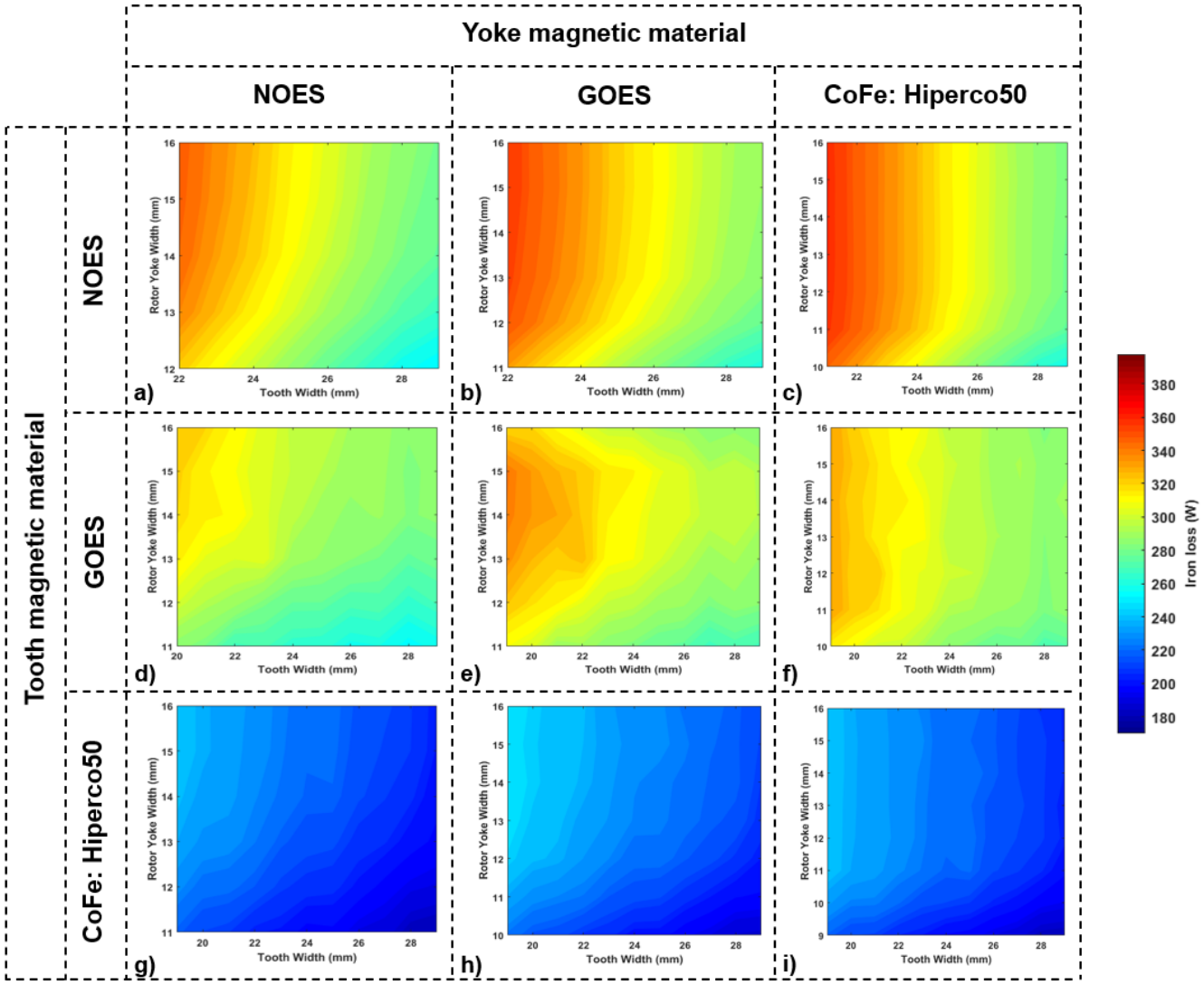

Fig.7. Variation of iron losses as a function of the tooth width and the yoke width for: a) Tn-Yn, b) Tn-Yg, c) Tn-Yh, d) Tg-Yn, e) Tg-Yg, f) Tg-Yh, g) Th-Yn, h) Th-Yg, i) Th-Yh

D. Efficiency optimization:

The use of different non-conventional materials in the magnetic circuit (stator and rotor) can also improve the efficiency of the electric motor. To do that, a mono-objective optimization for different structures as a function of geometrical dimensions (tooth width, yoke width) is performed. Results are given in Fig. 8. The maximum efficiencies obtained for each motor are given

in Table VII whereas the differences between the 3D and 2D calculations are given in Table VIII. The following conclusions can be written:

- The GOES in the rotor yoke is not advantageous, because the losses in the rotor increase; so this configuration is not adapted to this structure.
- On the other hand, using GOES in the stator leads to a strong improvement of the maximum efficiency with a benefit of more than 0.06%, compared to the NOES structure.
- Hiperco50 in the teeth allows to obtain a better improvement of the efficiency. The best structures in term of efficiency improvement are:
  - the mixt Hiperco50 tooth – NOES yoke structure (Th-Yn), with 25mm tooth width and 16mm yoke width, with an improvement of 0.10% compared to the NOES reference structure;
  - the full Hiperco50 structure (Th-Yh), with 24mm tooth width and 15mm yoke width, with a 0.11% improvement.

These improvements are small and it would be difficult to confirm them by practical measures.

From Table VIII, it can be seen that the average efficiency difference varies from 0.20% for the Th-Yn and Th-Yh structures up to 0.25% for the Tn-Yh structure. The 2D results are always underestimated compared to the 3D calculation. The overall average difference for the 257 simulation cases is 0.22%. That's particularly low, which validate the results obtained in 2D. It should be noted that the differences for the structures including the GOES sheet could not be performed, due to the divergence of the iron losses in 3D, such a calculation combining stauration and anisotropy to estimate the losses is still challenging.

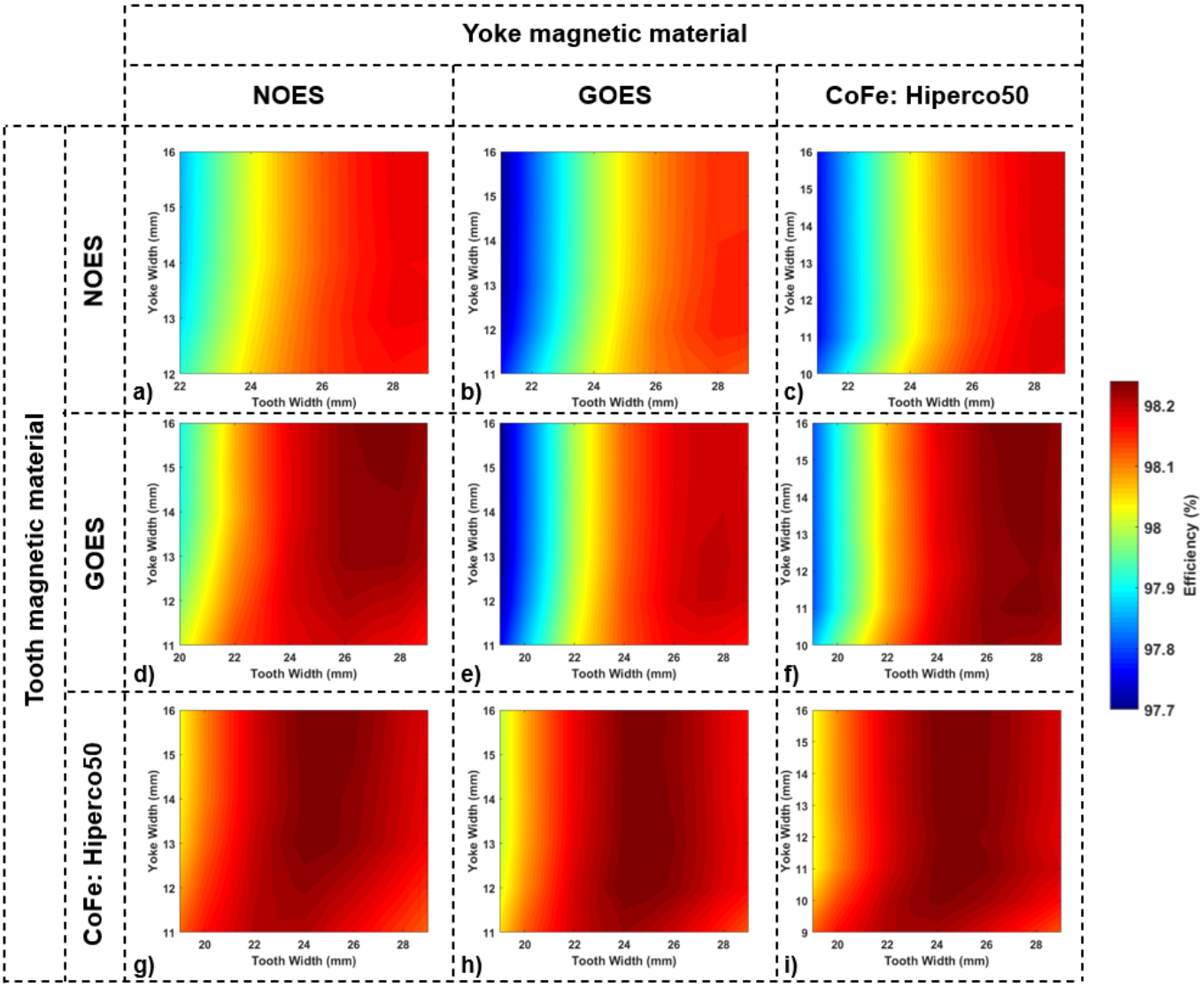

Fig.8. Variation of the efficiency as a function of the tooth-width and the yoke-width for: a) Tn-Yn, b) Tn-Yg, c) Tn-Yh, d) Tg-Yn, e) Tg-Yg, f) Tg-Yh, g) Th-Yn, h) Th-Yg, i) Th-Yh

TABLE VII
MAXIMAL EFFICIENCY AND IMPROVEMENT

Structures	Max efficiency (%)	Improvement (%)
Tn-Yn	98.14	-
Tn-Yg	98.11	-0.03
Tn-Yh	98.15	0.01
Tg-Yn	98.20	0.06
Tg-Yg	98.16	0.02
Tg-Yh	98.21	0.07
Th-Yn	98.24	0.10
Th-Yg	98.15	0.01
Th-Yh	98.25	0.11

TABLE VIII
DIFFERENCE BETWEEN THE FEA-3D AND FEA-2D

Structures	Minimum difference (%)	Maximum difference (%)	Average difference (%)	Number of simulation cases
Tn-Yn	0.17	0.31	0.23	40
Tn-Yg	-	-	-	54
Tn-Yh	0.17	0.36	0.25	63
Tg-Yn	-	-	-	60
Tg-Yg	-	-	-	66
Tg-Yh	-	-	-	77
Th-Yn	0.14	0.26	0.20	66
Th-Yg	-	-	-	66
Th-Yh	0.14	0.26	0.20	88

E. Multi-objective optimization:

A multi-objective optimization has been applied in order to design the optimal structure. This multi-objective optimization is based on the genetic algorithm NSGA2 (Non-dominated Sorting Genetic Algorithm) implemented in JMAG software application. The optimization objectives concern the power density and efficiency maximization, depending on the different magnetic materials and on the teeth and yoke geometric dimensions. The flowchart of the simulation and optimization process is given in Fig.9. Tables IX, X, and XI give respectively the optimization parameters and their range, the optimization constraints, and the optimization tool parameters of NSGA2.

TABLE IX
OPTIMIZATION VARIABLES

Parameters	Range
Tooth width (mm)	[1, 10]
Yoke width (mm)	[10, 50]
Magnetic materials	NOES, GOES, Hiperco50

TABLE X
OPTIMIZATION CONSTRAINTS

Optimization Constraints	Min Value	Max Value
Power (kW)	90	105
Induced voltage (V)	-	$\frac{800}{\sqrt{3}}$

TABLE XI
OPTIMIZATION TOOL PARAMETERS

Parameters	Number of individuals	Number of generations	Number of variables	Number of constraints	Number of objectives
Values	100	50	3	2	2

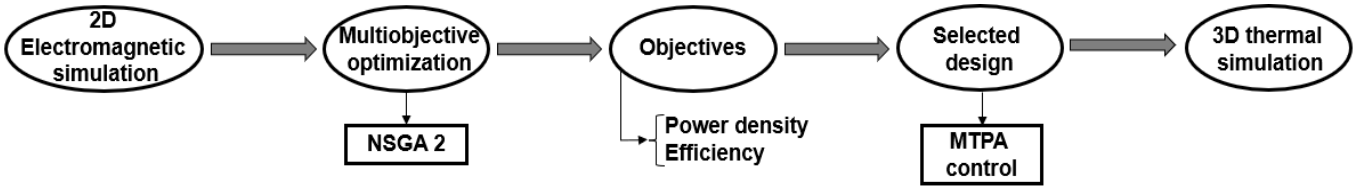

Fig. 9. Flowchart of the simulation and optimization process

Fig. 10 shows the Pareto fronts for the 9 structures described in Table III. The use of non-conventional magnetic materials, with full or mixed structures, always allows to improve the performances of the electric motor in terms of power density and efficiency, except for the structure with NOES conventional teeth and GOES yoke (Tn-Yg) for which only the power density is improved. The top three improved structures in power density and/or efficiency are:

- the full Hiperco50 structure (Th-Yh);
- the mixed GOES teeth - Hiperco50 yoke structure (Tg-Yh);
- the mixed Hiperco50 teeth - NOES yoke structure (Th-Yn).

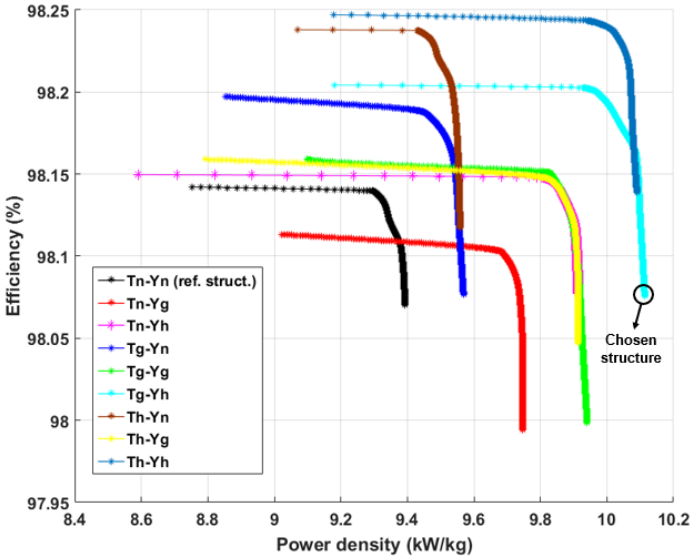

Fig.10. Variation of the optimization criteria (Pareto front)

F. Performance of the selected motor:

The mix GOES teeth - Hiperco50 yoke structure (Tg-Yh) is chosen for our motor, with a yoke width of 10mm and a tooth width of 22mm (Table XII). It has been selected from the Pareto front (Fig. 11) and it provides the maximal power density of 10.11kW/kg and an efficiency of 98.08% at 10000rpm and a 130Arms current.

TABLE XII
OPTIMAL DATA OF THE SELECTED DESIGN

Parameters	Value
Tooth width (mm)	22
Yoke width (mm)	10
Magnetic materials in stator	GOES
Magnetic materials in rotor	Hiperco50

The efficiency of the chosen motor at different operating points in the torque-speed plane is shown in Fig. 9. It is plotted for both operating modes: constant torque and flux weakening, using the MTPA control strategy. The map is calculated by FEA considering the iron losses, eddy current losses in the magnets and Joule losses considering coil-ends and the skin effect/proximity effect (*Rebhaoui et al., 2022a*). The structure has a very high efficiency in the constant torque operating range (98.38%). It degrades with the flux weakening when the speed increases and at low load (89.57%). This is due to the increase in iron losses, losses in the permanent magnets and Joule effect losses at high frequency.

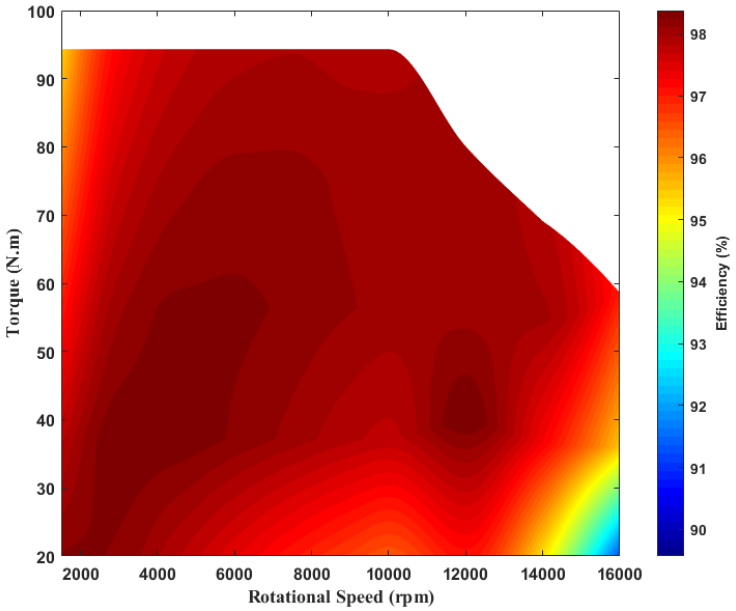

Fig.11. Efficiency maps of the selected motor

G. Thermal behavior of the selected motor:

Excessive temperatures reduce the motor life by damaging the winding insulation and demagnetizing the permanent magnets.. Losses in the windings, in the iron and in the magnets act as heat sources that increase the motor temperature. The steady-state thermal study has been performed using Altair Flux3D software application, version 2022.1. The assumptions made to perform the thermal modelling are the following:

- the radiation effects and the mechanical losses are neglected;
- constant volume losses in the elements are considered;
- the geometries of the bearings and stator cooling are simplified;
- the thermal conductivities of each material in the machine are given in the table XIII;
- the losses in each part of the machine are given in Table XIV;
- the geometry, divided in two parts with respect to the symmetry plane, is meshed with 4 559 102 elements. The stator windings and rotor yoke are water-cooled. The stator cooling flow is 12l/min, and the rotor cooling flow is 6l/min. The convective heat transfer coefficients, given in the table XV, are obtained by CFD (Computational Fluid Dynamics) simulations in Ansys Fluent application, version 2022R1.

Thermal simulation results in the active parts (windings, teeth, magnets, and rotor yoke), the housing and the shaft are given in figure 12. The maximum temperature of 148°C can be observed in the stator winding as Joule losses are the highest in the machine. That means that conventional organic insulation is sufficient and that current density could be slightly increased. In the stator teeth, an average temperature of 140°C is reached (Fig.12-a). The maximum temperature in the rotor yoke is 104C and 124°C the magnets, which is acceptable for Samarium Cobalt Magnets, as this type of magnets can work up to 300°C (Fig.12-b). Fig.12-c shows that the maximum temperatures reached in the housing and shaft are equal to 107°C and 90°C respectively. This first analyze shows that the designed cooling system keeps the electrical insulation system and the magnets under the temperature limits. The authors plan to increase the current density to improve the power density.

TABLE XIII
THERMAL CONDUCTIVITY

	Value (W/(m.K))
Hiperco50	29
GOES	29
Sm_2Co_{17}	15
Aluminum	200
Copper	380
Steel	50

TABLE XIV
LOSSES IN THE ACTIVE PARTS

Types losses	Value (W)
Joule losses	938,77
Iron losses in the stator	309.21
Iron losses in the rotor yoke	5.50
Magnet losses	396

TABLE XV
HEAT TRANSFER COEFFICIENTS

	Value (W/(m².K))
Housing	30
shaft	30
Teeth	30
Windings	4500
Rotor Yoke	3000
PM	30

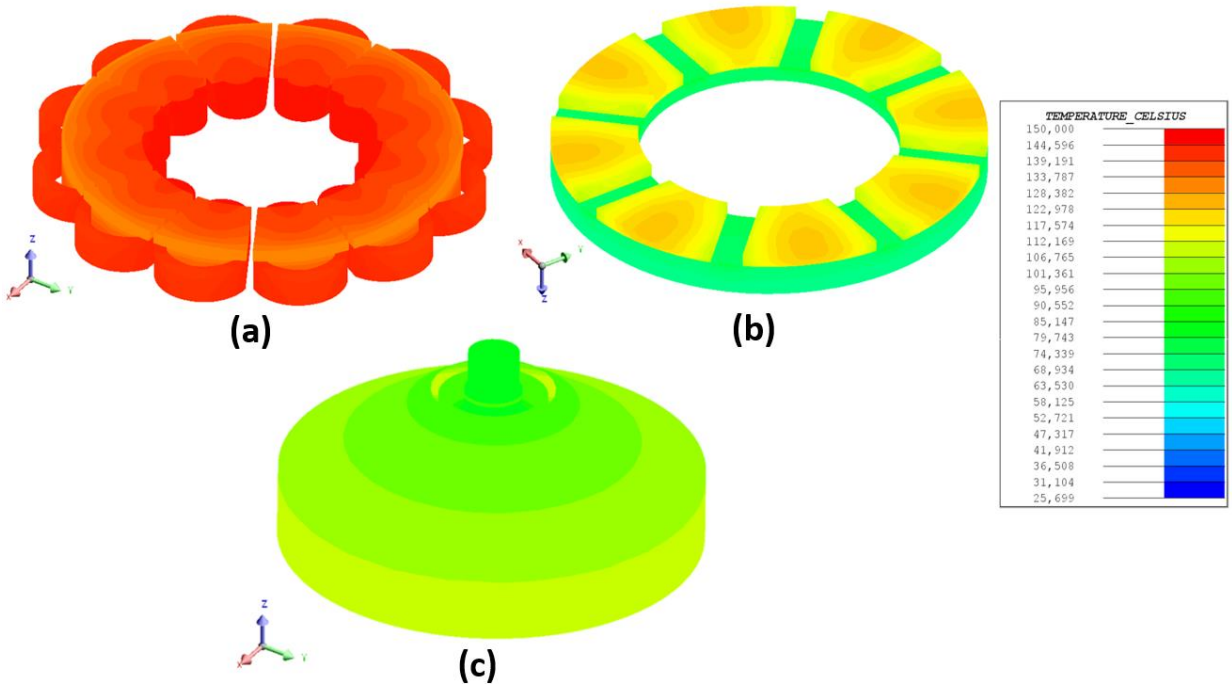

Fig.12. The temperature distribution in the: (a) winding and teeth, (b) Rotor yoke and magnets, (c) housing and shaft

V. CONCLUSION

In this paper, the effects of using different magnetic materials (NOES, GOES and Hiperco50) in the magnetic circuit (stator-rotor) of a 12-tooth-pole dual-rotor and yokeless-stator PMSM axial flux machine, are numerical analysed in order to improve the power density and the efficiency. The study is based on FEA-2D numerical modelling of the machine at the average radius and at the rated operating point. The comparison between the 2D and 3D calculation showed very good results in terms of power calculation with an average difference of 2.07%. For the calculation of the iron losses, the average difference is 10.8%. For pre-sizing, the 2D model is highly suitable. However, it remains limited, for example, an analysis of the impact of the internal or external radius cannot be performed. The principle of the study is to integrate different materials in the magnetic circuit, which gives full or mixed structures in the rotor and the stator. Mono-objective/multi-objective optimizations are performed for an optimal design with the goal of improving power density and/or efficiency by varying the geometrical dimensions of the stator teeth and the rotor yoke.

GOES in the stator teeth and Hiperco50 in the stator teeth and/or in the rotor yoke can improve power density and efficiency simultaneously, compared to a conventional NOES structure. The best structures in terms of power density and/or efficiency are:

- the GOES teeth - Hiperco50 yoke structure for the best power density;
- the mixt of Hiperco50 teeth and NOES yoke for high efficiency;
- the full Hiperco50 structure to get high power density and the best performance.

The GOES teeth - Hiperco50 yoke structure, which has the highest power density (10.11kW/kg), has been chosen to evaluate its efficiency in the torque-speed plane. The maximum efficiency of this structure can reach a high value of 98.38% at low average speed-load. This efficiency decreases with increasing speed. These conclusions result from numerical calculations based on implemented models. The latter may suffer from intrinsic errors, as the loss model or the anisotropic model for GOES.

The temperatures obtained in the active parts lead the authors to think of increasing the current density further. However, the losses need to be evaluated experimentally and to consider coupling the thermal and magnetic model.

For future work, experimental tests on a prototype motor will be performed.

VI. REFERENCES

Amin, S., Khan, S., & Hussain Bukhari, S. S. (2019). A Comprehensive Review on Axial Flux Machines and Its Applications. 2019 2nd International Conference on Computing, Mathematics and Engineering Technologies (ICoMET), 1–7. https://doi.org/10.1109/ICOMET.2019.8673422

ArcelorMittal Electrical steels - Industry. (2022.). from https://industry.arcelormittal.com/electricalsteels

Bhagubai, P. P. C., & Fernandes, J. F. P. (2020). Multi-Objective Optimization of Electrical Machine Magnetic Core Using a Vanadium–Cobalt–Iron Alloy. IEEE Transactions on Magnetics, 56(2), 1–9. https://doi.org/10.1109/TMAG.2019.2950880

Bloch, F., Waeckerle, T., & Fraisse, H. (2007). The use of iron-nickel and iron-cobalt alloys in electrical engineering, and especially for electrical motors. 2007 Electrical Insulation Conference and Electrical Manufacturing Expo, 394–401. https://doi.org/10.1109/EEIC.2007.4562649

Borisavljevic, A. (2013). Limits, Modeling and Design of High-Speed Permanent Magnet Machines. Springer Berlin Heidelberg. https://doi.org/10.1007/978-3-642-33457-3

Campbell, P. (1974). Principles of a permanent-magnet axial-field d.c. machine. Proceedings of the Institution of Electrical Engineers, 121(12), 1489. https://doi.org/10.1049/piee.1974.0311

Carpenter Electrification. (2022). from https://www.carpenterelectrification.com/products/soft-magnetic-alloy

Chan, C. C. (2002). The state of the art of electric and hybrid vehicles. Proceedings of the IEEE, 90(2), 247–275. https://doi.org/10.1109/5.989873

Dominique Auverlot, Nicolas Meilhan, Bérengère Mesqui, & Aude Pommeret. (2018). Les politiques publiques en faveur des véhicules à très faibles émissions (France stratégie).

Dwivedi, S. K., Singh, B., & Singh, B. P. (2006). A State of Art on Different Configurations of Permanent Magnet Brushless Machines. https://doi.org/10.13140/RG.2.1.2639.7929

Fujisaki, K. (2019). Magnetic Material for Motor Drive Systems (K. Fujisaki, Ed.). Springer Singapore. https://doi.org/10.1007/978-981-32-9906-1

Gieras, J. F., Wang, R.-Jie., & Kamper, M. J. (2008). Axial flux permanent magnet brushless machines. Springer.

Hanselman Duane. (1994). Brushless Permanent Magnet Motor Design Second Edition (Mcgraw-Hill).

JMAG. (2022). from https://www.jmag-international.com/

Koua Malick Cisse, Sami Hlioui, Yuan Cheng, & M'Hamed Belhadi. (2018). Etat de l'art des topologies de machines électriques utilisées dans les véhicules électriques et hybrides. https://hal.archives-ouvertes.fr/hal-02981853

Kowal, D., Sergeant, P., Dupré, L., & van den Bossche, A. (2010). Comparison of nonoriented and grain-oriented material in an axial flux permanent-magnet machine. IEEE Transactions on Magnetics, 46(2), 279–285. https://doi.org/10.1109/TMAG.2009.2032145

Laidoudi, A., Duchesne, S., Morganti, F., & Velu, G. (2020). High-power density induction machines with increased windings temperature. Open Physics, 18(1), 642–651. https://doi.org/10.1515/phys-2020-0131

Nagorny, A. S., Dravid, N. V., Jansen, R. H., & Kenny, B. H. (2005). Design aspects of a high speed permanent magnet synchronous motor / generator for flywheel applications. IEEE International Conference on Electric Machines and Drives, 2005., 635–641. https://doi.org/10.1109/IEMDC.2005.195790

Pyrhnen, J., Jokinen, T., & Hrabovcov, V. (2008). Design of Rotating Electrical Machines. John Wiley & Sons, Ltd. https://doi.org/10.1002/9780470740095

Rebhaoui, A., Randi, S. A., Demian, C., & Lecointe, J.-P. (2022a). Using grain oriented electrical steel sheets for electric motor in automotive application: Tooth segmentation. International Journal of Applied Electromagnetics and Mechanics, 69(2), 221–232. https://doi.org/10.3233/JAE-210186

Rebhaoui, A., Randi, S. A., Demian, C., & Lecointe, J.-Ph. (2022b). Analysis of Flux Density and Iron Loss Distributions in Segmented Magnetic Circuits Made With Mixed Electrical Steel Grades. IEEE Transactions on Magnetics, 58(8), 1–11. https://doi.org/10.1109/TMAG.2021.3138984

Rezzoug, Abderrezak., & el Hadi Zaïm, Mohamed. (2012). Non-conventional electrical machines. ISTE.

thyssenkrupp Steel Europe. (2022). from https://www.thyssenkrupp-steel.com/en/company/business-units/electrical-steel/

Zhu, Z. Q., & Howe, D. (2007). Electrical machines and drives for electric, hybrid, and fuel cell vehicles. Proceedings of the IEEE, 95(4), 746–765. https://doi.org/10.1109/JPROC.2006.892482